The Hydrogen-Containing Bronzes $H_{0.23}WO_3$ and $H_{0.10}ReO_3$ Synthesized via a Polymer Route

Lun Jin [a], Qiang Zhang [b] and Robert J. Cava*[a]

[a] Department of Chemistry, Princeton University, Princeton, New Jersey 08544, USA

[b] Neutron Scattering Division, Oak Ridge National Laboratory, Oak Ridge, Tennessee 37831, USA

Abstract

We report the synthesis of two hydrogen-containing perovskite-type bronzes $H_{0.23}WO_3$ and $H_{0.10}ReO_3$ utilizing an unconventional solid-state synthetic approach, involving the use of the polymer Poly(vinylidene fluoride) $(CH_2CF_2)_n$. Powder neutron diffraction at ambient temperature shows that $H_{0.23}WO_3$ crystallizes in a tetragonal symmetry distortion of the simple perovskite structure (space group *P*4/*nmm*), with lattice parameters a = 5.2279(2) Å, and c = 3.8763(1) Å. $H_{0.10}ReO_3$, in contrast, crystallizes in a monoclinic distortion of a simple cubic perovskite (space group *P*2/*m*), with lattice parameters a = 5.3125(1) Å, b = 5.3155(3) Å, c = 3.7045(3) Å, and γ = 90.43(1)°. Both $H_{0.23}WO_3$ and $H_{0.10}ReO_3$ exhibit intrinsically diamagnetic behavior, with low temperature paramagnetic upturns and no signs of bulk superconductivity down to 0.35 K.

Keywords: Hydrogen-containing perovskite-type bronzes; Polymer route; Poly(vinylidene fluoride); X-ray powder diffraction; neutron powder diffraction; diamagnetic.

1. Introduction

Transition-metal oxides continue to be the subject of extensive study because they exhibit a wide variety of interesting chemical and physical properties. The bronze family, as an important sub-group of transition-metal oxides, contains a large variety of nonstoichiometric ternary oxides that have the general formula A_xMO_3 ($0 < x < 1$). A is usually an electropositive element that can donate electrons to the host network, which in many cases solely consists of corner-sharing MO_6 octahedra. The three-dimensional network of MO_6 octahedra shows good tolerance to accommodate different dopants in its cavities such as elements of group 1, 2, 13, 14, 15, lanthanides, and actinides.[1–18]. In addition, the choice of the transition-metal M can vary from W, which has been intensively studied, to other less well-characterized materials based on Mo, Nb, Ta, Re and V[19–31]. Therefore, this family of materials has very rich chemistry and forms a large variety of distinct structural types. In general, the crystal structures can be broadly classified as the perovskite tungsten bronze type (PTB), the tetragonal tungsten bronze type (TTB), the hexagonal tungsten bronze type (HTB) and the intergrowth tungsten bronze type (ITB). This family of materials attracts enduring interest for its potential applications in electrochromic technology, photocatalysis, dye-sensitized solar cells, solar water-splitting and plasmonic materials[32–35]. In addition, their capability to host interesting physical properties such as superconductivity, magnetic ordering, and ferroelectricity makes them a keen research topic in fundamental scientific research[1,2,4–6,8,12,20,36–43].

In the course of developing the bronze family, different methods have been used to prepare them, with the most versatile method being solid-state reaction. Bronzes with the usual dopants in the cavities such as alkali metals can be easily made by mixing stoichiometric amounts of starting materials and sintering at appropriate temperatures[1,43,44]. In contrast, some unusual dopants

require more complicated techniques to be intercalated, such as high pressure[18], hydrothermal synthesis[11] or a metal halide route[3,45,46] to obtain otherwise difficult bronzes. The formation of $WO_{3-x}F_x$ ($x \leq 0.45$), prepared via a chemically reducing fluorination route, using the polymer polytetrafluoroethylene (Teflon) to react with WO_3[47], shows that the parent M_xO_y phases are not inert to polymers. Since hydrogen is not only a common element in some polymers such as poly(vinylidene fluoride), $(CH_2CF_2)_n$ and polyethylene $(CH_2CH_2)_n$, but also an unusual dopant in the bronze family, modification of the parent M_xO_y phases with appropriate hydrogen-containing polymers, either by intercalating H^+ into cavities to form bronzes, or by partial hydride-for-oxide substitution to form mixed-anion compounds, should be feasible.

In this work, WO_3, ReO_3, MoO_3, Nb_2O_5, Ta_2O_5, V_2O_5 and TiO_2 were selected as starting materials for testing their reactivity with the hydrogen-containing polymer Poly(vinylidene fluoride), $(CH_2CF_2)_n$ (PVDF), but it was found that only WO_3 and ReO_3 allow for the intercalation of H^+ into their cavities to form bronzes by this method. H_xWO_3 has previously been reported to crystallize in orthorhombic symmetry for $x = 0.10$, tetragonal symmetry for $x = 0.23$ and 0.33, and cubic symmetry for $x = 0.50$ and 0.53[15,48,49], while H_xReO_3 has been reported to crystallize in orthorhombic symmetry for $x = 0.15$, 0.25 and 0.38, tetragonal symmetry for $x = 0.81$, and cubic symmetry for $x = 1.36$ and 1.40[28,29,31,50]. Although H_xMoO_3 ($0 < x \leq 2.0$)[30] has also been reported, we found that the MoO_3 lattice is too vulnerable to survive under the reducing conditions created by the PVDF powder. The methods used to prepare hydrogen-containing bronzes in the literature all employ aqueous conditions, such as water[31], hydrochloric acid[15,30,48], sulfuric acid[29] and chloroplatinic acid followed by exposure to hydrogen gas[28,29]. Our polymer route provides an alternative, purely solid-state approach to synthesize the hydrogen-containing tungsten and rhenium bronzes, without the interference of aqueous reaction conditions and following

purification procedures. The reactions occur at the gas-solid interface. PVDF begins to decompose at 150 °C and evaporates into its gaseous-state monomer VDF under vacuum around the reaction temperature of 350 °C, which fills the reaction vessel and reacts with WO_3 or ReO_3. The actual protonation reaction mechanism is not known, as the H-depleted products of the secondary reactions of gaseous VDF have not been determined.

Thus, here we report the successful synthesis of two hydrogen-containing perovskite-type bronzes $H_{0.23}WO_3$ and $H_{0.10}ReO_3$ via a solid-state polymer-based synthetic approach, involving the use of Poly(vinylidene fluoride) $(CH_2CF_2)_n$ powder. To the best of our knowledge, no previous reports of bronzes prepared by this method can be found in the literature. Since the positions of light elements, in this case, hydrogen and oxygen, cannot be well specified by X-ray diffraction in the presence of the heavy elements tungsten and rhenium, we employ neutron powder diffraction to fully characterize their crystal structures. Both the crystal structures and hydrogen contents of $H_{0.23}WO_3$ and $H_{0.10}ReO_3$ are determined by the analysis of Time-of-Flight (TOF) neutron powder diffraction data in this study. In addition to the structural chemistry, the magnetic properties of these two bronzes are characterized.

2. Experimental

Polycrystalline powder samples of the two hydrogen-containing perovskite-type bronzes $H_{0.23}WO_3$ and $H_{0.10}ReO_3$ were synthesized by an approach involving the use of polymer Poly(vinylidene fluoride) powder, which is a vapor at the temperatures employed. The reactions occurred at the gas-solid interface. Approximately 200 mg of starting materials WO_3 (Alfa Aesar, 99.8%) and ReO_3 (Alfa Aesar, 99.9%) were mixed and ground with 100 mg of PVDF powder, and then the resulting mixtures were sealed in evacuated quartz tubes. The reaction vessels were heated

at 350 °C for 7 days. The purity, symmetry, and unit cell parameters of the resulting samples were examined by laboratory X-ray powder diffraction data collected at room temperature on a Bruker D8 FOCUS diffractometer (Cu Kα) over a 2θ range between 5° and 70°. Lattice parameters, atomic positions, and atomic displacement factors were initially determined and refined by the Rietveld method using the GSAS-II program.

The large-scale polycrystalline powder samples of $H_{0.23}WO_3$ and $H_{0.10}ReO_3$ for the neutron diffraction experiments were synthesized by reacting approximately 2 g of the starting materials WO_3 (Alfa Aesar, 99.8%) and ReO_3 (Alfa Aesar, 99.9%) with 1 g of PVDF powder. The sealed evacuated quartz tubes containing the samples were heated at 350 °C for two to three periods of 7 days, with the samples being reground and a suitable amount of PVDF powder re-added between heating periods. Routine inspections of reaction mixtures after each heating period were performed by laboratory X-ray powder diffraction to ensure the completion of the reactions and the homogeneity of the neutron samples. Time-of-flight (TOF) neutron powder diffraction data were collected for $H_{0.23}WO_3$ and $H_{0.10}ReO_3$ at Oak Ridge National Laboratory's (ORNL's) Spallation Neutron Source (SNS) POWGEN beamline using a beam of neutrons with a center wavelength of 0.8 Å, at both 300 K and 7 K. Lattice parameters, atomic positions, and atomic displacement factors were refined by the Rietveld method using the GSAS-II program.

To chemically prove that the intercalated element in the tunnels is hydrogen rather than fluorine, similar reactions were performed on the starting materials WO_3 (Alfa Aesar, 99.8%) and ReO_3 (Alfa Aesar, 99.9%), but with the PVDF powder replaced by Polyethylene $(CH_2CH_2)_n$ powder. Laboratory X-ray powder diffraction indicated that identical reaction products were formed. The texture of resulting products was gel-like, however, which made them unsuitable for detailed analysis compared to the loose powder products formed by using PVDF powder.

The temperature-dependent magnetization data for $H_{0.23}WO_3$ and $H_{0.10}ReO_3$ were collected using the vibrating sample magnetometer (VSM) option of a Quantum Design Physical Property Measurement System (PPMS). Temperature-dependent magnetization data were collected from finely ground $H_{0.23}WO_3$ and $H_{0.10}ReO_3$ powders in an applied field of 1000 Oe, and field-dependent magnetization data between H = 90000 Oe. and –90000 Oe. were collected from the samples at T = 300 K and 2 K.

The potential for bulk superconductivity of $H_{0.23}WO_3$ and $H_{0.10}ReO_3$ was tested on a small amount of powder in the Quantum Design Physical Property Measurement System (PPMS) down to 1.7 K in an applied magnetic field of 10 Oe. For the lower temperature regime (T < 1.7 K), specific-heat measurements down to 0.35 K were performed in the PPMS equipped with a ^{3}He insert to test for whether the entropy change expected to accompany an electronic phase transition is present.

3. Results and Discussion

3.1 Structural Characterization

$H_{0.23}WO_3$ is a perovskite-type tungsten bronze (PTB) that crystalizes in the tetragonal symmetry system, with the A-site of the perovskite partially occupied by H^+. Standard laboratory X-ray powder diffraction (XRD) data collected from the fine black $H_{0.23}WO_3$ powder obtained by reacting WO_3 with PVDF, can be roughly indexed by a tetragonal unit cell, with lattice parameters of a = 5.22 Å, c = 3.88 Å, which is in good agreement with the literature[15]. In addition, higher sensitivity XRD data collected from the same sample in air shows the conversion of the tetragonal product $H_{0.23}WO_3$ back to the monoclinic starting material WO_3, which reflects the air-sensitive nature of this material. The atomic position and site fraction of H^+ in the tunnel of the WO_3 array, which consists of corner-sharing WO_6 octahedra, was confirmed by refining the ambient TOF

neutron powder diffraction data against the reported structural model of $H_{0.23}WO_3$[15]. The refinement converged smoothly and provides a satisfactory agreement parameter (*wR* = 2.94%; *GOF* = 2.38). Observed, calculated and difference plots from the Rietveld refinement of $H_{0.23}WO_3$ (space group *P*4/*nmm*) based on the ambient neutron powder diffraction data are shown in Figure 1(a). The structural model of $H_{0.23}WO_3$ and selected bond lengths of the WO_6 octahedron and the H-O polyhedron are depicted in Figure 1(b). Detailed structural parameters and crystallographic positions are presented in Table 1. Neutron powder diffraction data collected from $H_{0.23}WO_3$ at lower temperature reveals no additional structural features. Details can be found in the Supporting Information (SI).

The laboratory X-ray powder diffraction (XRD) data collected from the fine black powder $H_{0.10}ReO_3$, obtained by reacting ReO_3 with PVDF, could be roughly indexed by an orthorhombic unit cell, with lattice parameters of *a* = 3.77 Å, *b* = 3.74 Å, *c* = 3.70 Å, which is in a good agreement with the literature[31]. In contrast to the W analogue, higher sensitivity XRD data collected from this sample while exposed to air is identical to the initial scan, which indicates the air-stable nature of this material. The ambient neutron powder diffraction data collected from this compound was initially refined using a model based on the structural model of $H_{0.15}ReO_3$[31] previously reported. This model is constructed by a simple orthorhombic unit cell with the above-mentioned lattice parameters (space group *Pmmm*). The site fraction of H^+ in the tunnel, consisting of corner-sharing ReO_6 octahedra, was set to be 0.15 to start with, and let free to change afterwards. However, the refinement yielded unsatisfactory agreement parameters with poor visual fitting even after refining the site fraction of H^+ in the tunnel. Several strong peaks were not accommodated, plus poor fitting of some peak shapes was found, indicating there were some impurities in the sample. After considering the possible impurities, ReO_2 and Re, as partial decomposition products, stood out.

The refinement parameters when including those impurities were significantly improved (wR = 4.098%; *GOF* = 2.66). However, there remained a few peaks that cannot be accounted for by adding impurity phases, which made us question the validity of the orthorhombic structural model for our material.

Given that the XRD data can be easily indexed by the simple orthorhombic unit cell, while the neutron diffraction data reveals that some additional structural features must be present, it is reasonable to deduce that these features are due to the 'light' elements in the compound, hydrogen and oxygen. A new monoclinic unit cell (space group $P2/m$), as a result of $\sqrt{2} \times \sqrt{2} \times 1$ expansion of the original orthorhombic unit cell, was thus refined against the neutron powder diffraction data. By lowering the symmetry from orthorhombic to monoclinic and expanding the unit cell, possible tilting and distortion of ReO_6 octahedra (Figure 2(b)) can be introduced to the lattice, which successfully accounted for the peaks that could not be accommodated in the orthorhombic model. The refinement converged smoothly and provided satisfactory agreement parameters (wR = 3.475%; *GOF* = 2.34). The H content in our compound is finalized to be about 0.10, which is lower than the previously reported $H_{0.15}ReO_3$[31] orthorhombic bronze. Therefore, it is not surprising that our compound needs a lower symmetry unit cell to be fully described. Observed, calculated and difference plots from the Rietveld refinement of $H_{0.10}ReO_3$ (space group $P2/m$) against ambient neutron powder diffraction data are shown in Figure 2(a). The structural model for $H_{0.10}ReO_3$, and selected bond lengths of the ReO_6 octahedron and the H-O polyhedron are depicted in Figure 2(b). Detailed structural parameters and crystallographic positions are presented in Table 2. Neutron powder diffraction data collected from $H_{0.10}ReO_3$ at low temperature reveals no additional structural features. Details can be found in the Supporting Information (SI).

3.2 Magnetic Characterization

The temperature-dependent magnetization data collected from both $H_{0.23}WO_3$ and $H_{0.10}ReO_3$, is plotted as magnetic susceptibility χ (M/H) against temperature T in Figure 3. The magnetic susceptibility consists of a relatively temperature-independent part ($25 < T / K < 300$) and a strongly temperature-dependent part ($1.8 < T / K < 25$). The bulk diamagnetic behavior of the samples mainly contributes to the relatively temperature-independent part, while the magnetic behavior below $T = 25$ K is due to the presence of dilute magnetic impurities. Hence, the magnetic susceptibility data in the range $1.8 < T / K < 25$ were fitted to the Curie-Weiss law ($\chi = C/(T - \theta) + K$), to yield values of $C = 1.42(3)\times10^{-3}$ cm^3 K mol^{-1}, $\theta = -0.05(6)$ K for $H_{0.23}WO_3$, and $C = 1.48(5)\times10^{-3}$ cm^3 K mol^{-1}, $\theta = +1.35(2)$ K for $H_{0.10}ReO_3$ respectively. The values of $\mu^2 = 0.011\ \mu_B$ for $H_{0.23}WO_3$, and $\mu^2 = 0.012\ \mu_B$ for $H_{0.10}ReO_3$ can be calculated from this data, and the values of $\mu_{eff} = 0.107\ \mu_B$ for $H_{0.23}WO_3$, and $\mu_{eff} = 0.109\ \mu_B$ for $H_{0.10}ReO_3$ are extracted. According to $\mu = g\sqrt{s\ (s+1)}$ where g is the gyromagnetic ratio and s is the sum of the spin quantum numbers of the electrons in the system, the fraction of the potential spin 1 impurity are calculated to be 3.77% for $H_{0.23}WO_3$, and 3.85% for $H_{0.10}ReO_3$ respectively. Although it is less likely, we cannot rule out the possibility that these positive magnetic responses in the low temperature regime are actually intrinsic, i.e. not coming from impurities. The field-dependent magnetization data collected from both $H_{0.23}WO_3$ and $H_{0.10}ReO_3$ are plotted as magnetic moment M against field H in Figure 3. The magnetization data collected at 300 K as a function of applied field is linear and passes through the origin, with a negative slope (more obvious in the W case), while analogous data collected at 2 K have positive slopes instead, consistent with the temperature-dependent data.

No signs of bulk superconductivity were observed from either $H_{0.23}WO_3$ or $H_{0.10}ReO_3$ in the low applied field magnetic susceptibility measurements down to 1.7 K and in specific-heat

measurements down to 0.35 K. Combining both the temperature-dependent and the field-dependent magnetization data collected from $H_{0.23}WO_3$ and $H_{0.10}ReO_3$ samples, it is valid to conclude that these two materials exhibit bulk diamagnetic behavior, with no magnetic transitions.

3.3 Phase Diagram of Hydrogen-Containing Tungsten and Rhenium Bronzes

H^+ is the smallest dopant in the bronze family, even smaller than the usual dopants Li^+ and Na^+, so it is not surprising that hydrogen-containing bronzes prefer to adopt a perovskite-type structure, since its cavity size is the smallest among the four general structural types of bronzes (PTB, TTB, HTB and ITB). However, perovskite-type bronzes can crystallize in different symmetry systems, such as monoclinic, orthorhombic, tetragonal and cubic. The decisive factor determining the symmetry of the product appears to be the doping level. The general rule, which can be concluded from compounds reported in literature, is that a decrease in the crystallographic symmetry of the structure usually accompanies decreased doping levels. Possible explanations of this phenomenon may be primarily "mechanical" – namely that lower levels of dopant always yield lower cavity occupancy, with the unit cell of the average structure therefore having a lower symmetry to accommodate local differences in structure, or electronic, in the sense that the electronic structure of the products at low doping yields a lower density of states for low symmetry structures. Theoretical analysis of the structures of perovskite bronzes that considers these factors would be of interest.

Both $H_{0.23}WO_3$ and $H_{0.10}ReO_3$ presented in this work are hydrogen-containing perovskite-type bronzes, but they crystallize in tetragonal and monoclinic symmetry respectively, which fit, in their own categories, the general rule mentioned above. In this context, the cubic crystal structure of pristine ReO_3 seems to be anomalous. The phase diagram of all the existing hydrogen-containing

perovskite-type tungsten and rhenium bronzes against different doping levels x is depicted in Figure 4. The two phases marked in red are the two bronzes presented in this work. Some well-known Li_xWO_3 and Na_xWO_3 tungsten bronzes are plotted as well for comparison[51–58].

WO_3 commonly adopts a monoclinic structure at ambient temperature and pressure, with the initial electron count per MO_3 unit of 0 (at $x = 0$). With elevated doping levels of electropositive elements in the tunnels, the electron count per MO_3 unit increases, hence yielding the monoclinic-orthorhombic-tetragonal-cubic structural transition. The boundaries (doping levels needed to cause the structural transitions) between these structural types vary depending on the different kinds of dopants in the tunnels, which can be seen, for example, when considering H^+, Li^+ and Na^+ in Figure 4. In contrast, ReO_3 commonly adopts a cubic structure at ambient temperature and pressure instead, with the initial electron count per MO_3 unit of 1 (at $x = 0$). But with elevated doping levels, the electron counts per MO_3 unit deviate from 1, the same monoclinic-orthorhombic-tetragonal-cubic structural transition occurs as well. Our $H_{0.10}ReO_3$, which has the lowest H^+ doping level ever reported within Re bronzes, completes the above-mentioned structural transition series by providing the first monoclinic material in the H-Re-O system. In addition, the H-Re-O system is more tolerant to H accommodation than the H-W-O system, exhibiting a significantly wider doping range for H^+. The lower doping limit is similar in both systems, but the upper doping limit in the H-Re-O system is nearly three times of that in the H-W-O system.

4. Conclusion

The successful synthesis of two hydrogen-containing perovskite-type bronzes $H_{0.23}WO_3$ and $H_{0.10}ReO_3$ in powder form was achieved by utilizing an unconventional solid-state synthetic

approach, involving the use of the polymer Poly(vinylidene fluoride) to intercalate H^+ into the W-O and Re-O systems according to the following equations:

$$0.23H^- \text{ (from } CH_2CF_2) + W^{+6}O_3 = H^+_{0.23}W^{+5.77}O_3 \text{ (+ } 0.23(CHCF_2)^-)$$

$$0.10H^- \text{ (from } CH_2CF_2) + Re^{+6}O_3 = H^+_{0.10}Re^{+5.90}O_3 \text{ (+ } 0.10(CHCF_2)^-)$$

(The formulas of the H-depleted polymeric products are not actually known - we represent them schematically in the above as $(CHCF_2)^-$.) By switching from PVDF powder to Polyethylene $(CH_2CH_2)_n$ powder, identical products were synthesized, but the gel-like texture of the products proved to be unsuitable for further analysis. The reactions occurred at the gas-solid interface, so no purification procedures were required to separate target compounds as long as the starting materials were fully reacted. The crystal structures and hydrogen contents of both bronzes were determined by TOF neutron powder diffraction data. $H_{0.23}WO_3$ is a perovskite-type tungsten bronze (PTB) that crystalizes in the tetragonal symmetry system, with the A-site of the perovskite partially occupied by H^+. Both the structural model (a simple tetragonal unit cell (space group *P*4/*nmm*) with lattice parameters of a = 5.2279(2) Å, c = 3.8763(1) Å), and the hydrogen content 0.23(1) of our $H_{0.23}WO_3$ compound are in good agreement with the literature[15]. In contrast, our $H_{0.10}ReO_3$ compound shows structural features that cannot be reproduced when using the reported orthorhombic structural model of $H_{0.15}ReO_3$[31] to index the neutron diffraction pattern. Hence a new monoclinic unit cell (space group *P*2/*m*, a = 5.3125(1) Å, b = 5.3155(3) Å, c = 3.7045(3) Å, γ = 90.43(1)°), a result of a $\sqrt{2} \times \sqrt{2} \times 1$ expansion of the original orthorhombic unit cell (space group *Pmmm*), is proposed to describe the crystal structure of our $H_{0.10}ReO_3$ compound. In addition, the hydrogen content of our compound is 0.10, which is lower than the reported $H_{0.15}ReO_3$[31]. Therefore, it is not surprising that our compound needs a lower symmetry unit cell to be properly described. Magnetization data collected from both $H_{0.23}WO_3$ and $H_{0.10}ReO_3$ suggests that these

two compounds exhibit bulk diamagnetic behavior, with no signs of superconductivity observed down to 0.35 K.

Supporting Information

The Supporting Information is available free of charge. The Time-of-Flight neutron powder diffraction data collected from both hydrogen-containing bronzes $H_{0.23}WO_3$ and $H_{0.10}ReO_3$ at 7 K is provided.

Acknowledgements

The research at Princeton University was supported by the US Department of Energy, Division of Basic Energy Sciences, grant number DE-FG02-98ER45706. A portion of this research used resources at the Spallation Neutron Source, a DOE Office of Science User Facility operated by the Oak Ridge National Laboratory.

Conflict of Interest

The authors declare no conflict of interest.

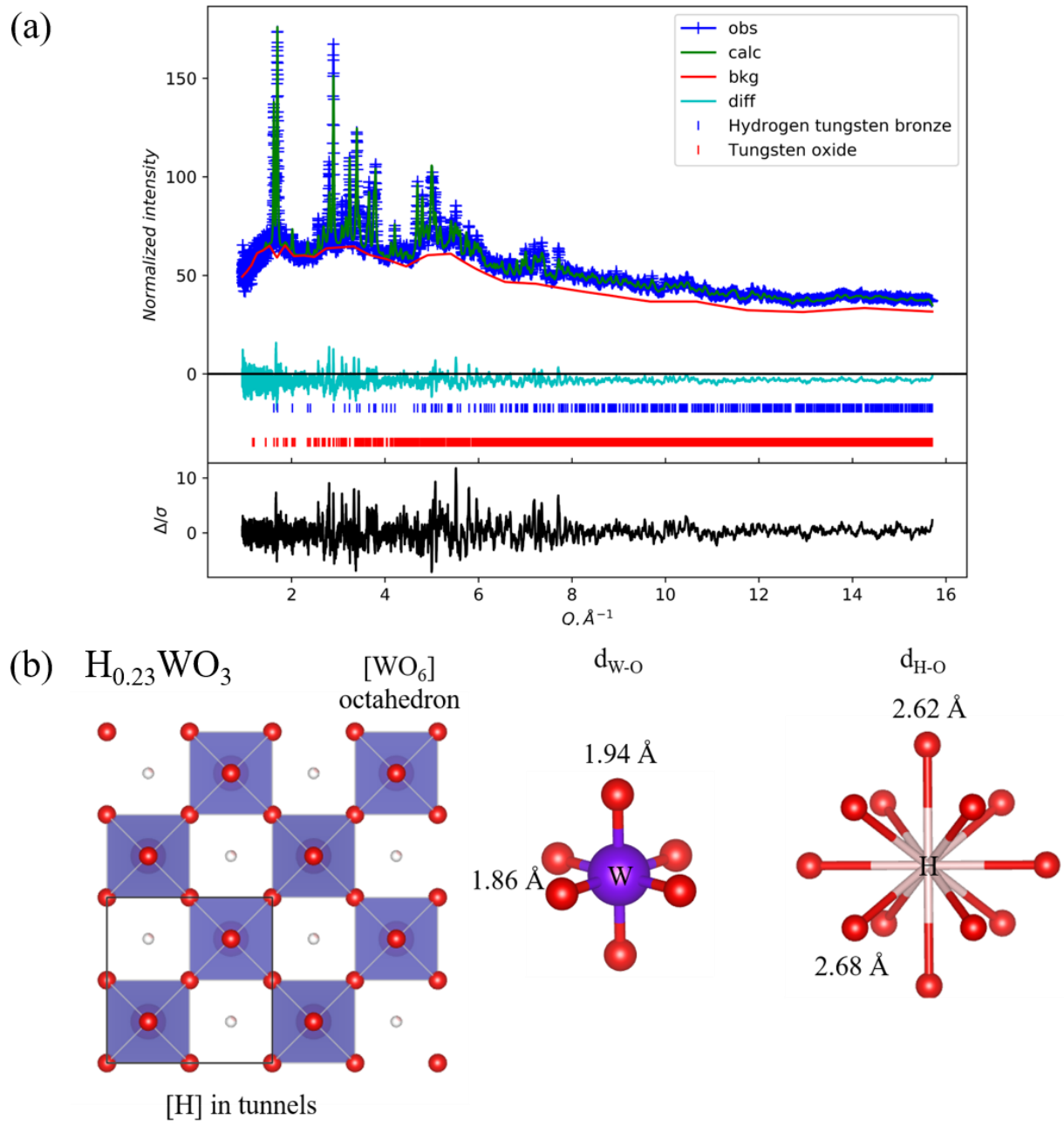

Figure 1. (a) Observed, calculated and difference plots from the Rietveld refinement of $H_{0.23}WO_3$ (space group *P*4/*nmm*) against ambient neutron powder diffraction data; (b) The structural model of $H_{0.23}WO_3$, and selected bond lengths of the WO_6 octahedron and the H-O polyhedron.

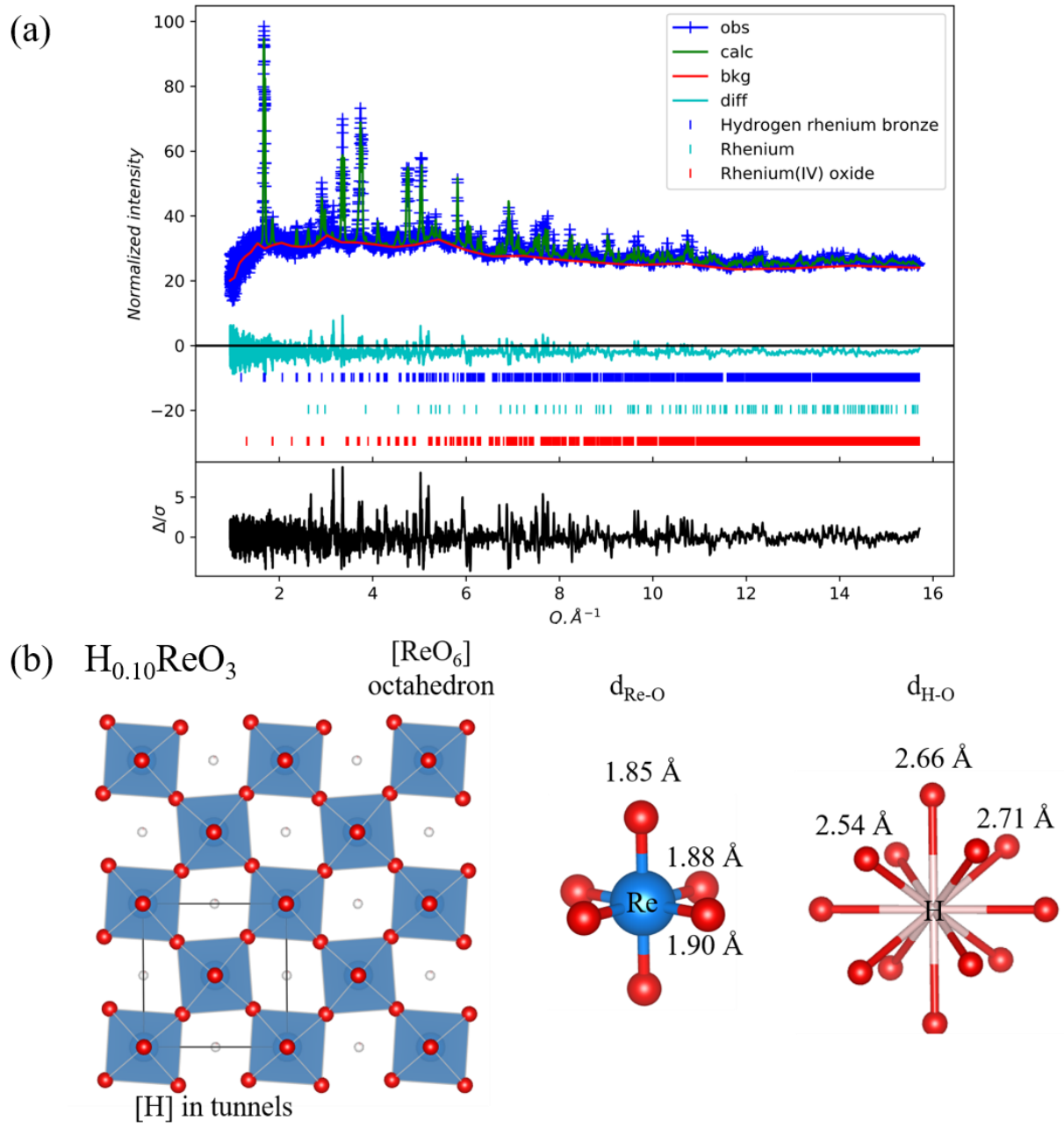

Figure 2. (a) Observed, calculated and difference plots from the Rietveld refinement of $H_{0.10}ReO_3$ (space group *P*2/*m*) against ambient neutron powder diffraction data; (b) The structural model of $H_{0.10}ReO_3$, and selected bond lengths of the ReO_6 octahedron and the H-O polyhedron.

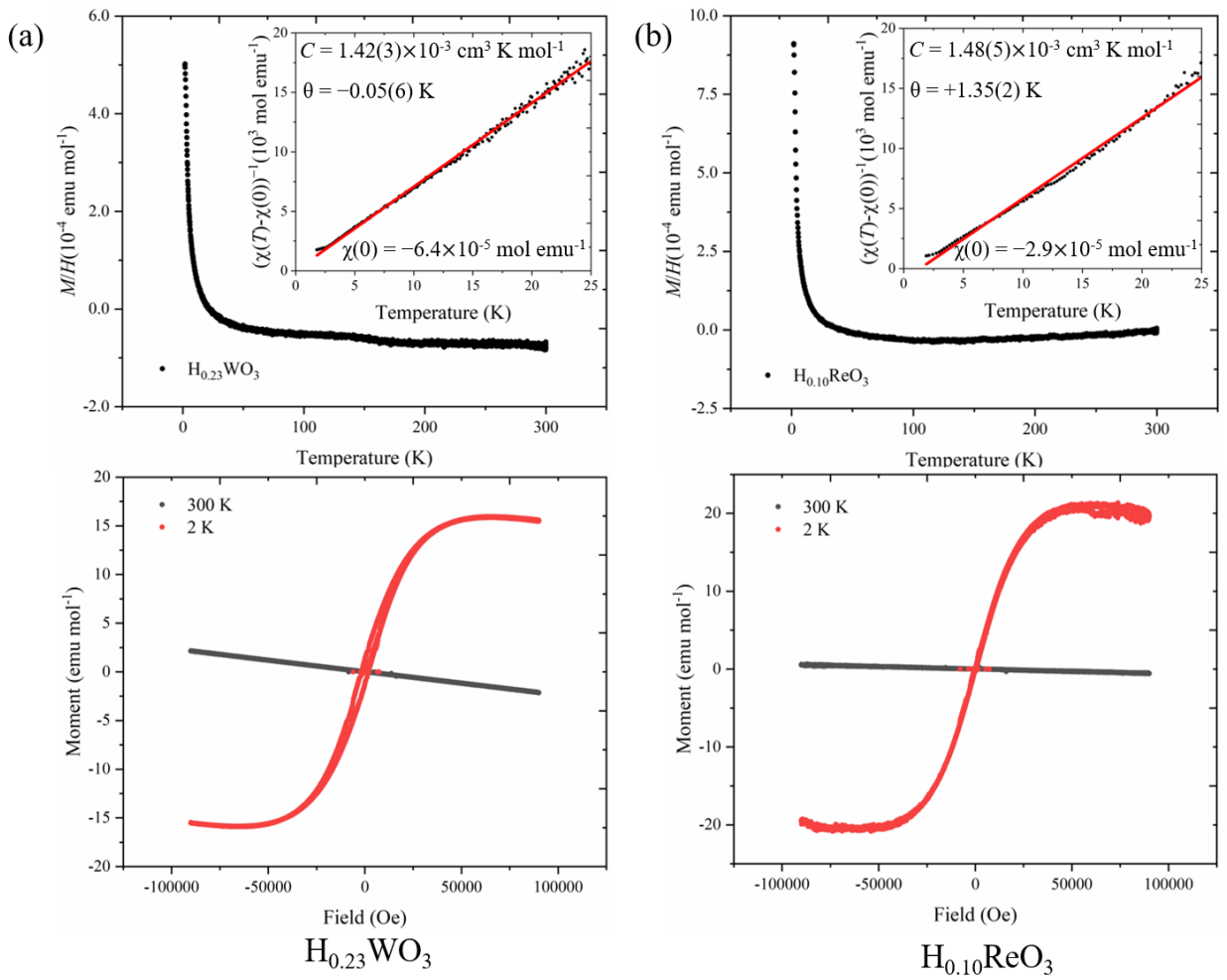

Figure 3. The magnetization data collected from (a) $H_{0.23}WO_3$ and (b) $H_{0.10}ReO_3$. The top panels are plotted as magnetic susceptibility χ (M/H) against temperature T, with $1/(\chi(T)- \chi(0))$ against T plots embedded; the bottom panels are plotted as magnetic moment M against field H.

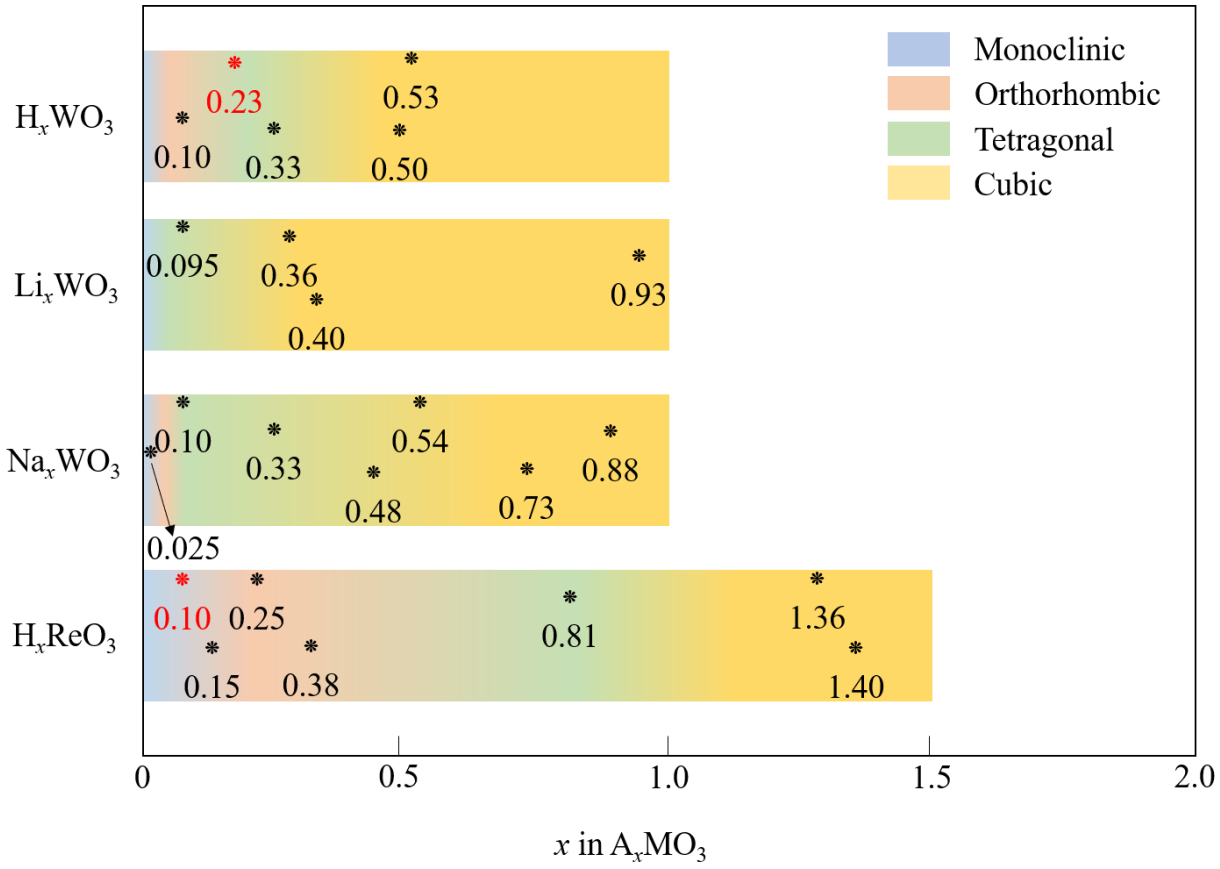

Figure 4. The four selected perovskite-type bronzes that crystallize in different symmetry system with respect to the doping level *x*. The phases marked in red are the two bronzes $H_{0.23}WO_3$ and $H_{0.10}ReO_3$ presented in this work.

Table 1. Structural parameters and crystallographic positions from the refinement of neutron powder diffraction data collected from $H_{0.23}WO_3$ at 300 K.

Atoms	x/*a*	y/*b*	z/*c*	S.O.F.	U_{iso} equiv. ($Å^2$)
W1	1/4	1/4	0.0259(2)	1	0.07254
O1	1/4	1/4	0.5769(3)	1	0.00283
O2	0	0	0	1	0.07644
H1	3/4	1/4	1/2	0.23(1)	0.01508

$H_{0.23}WO_3$ space group *P*4/*nmm* (#129)

Formula weight: 232.07 g mol^{-1}, Z = 2

a = 5.2279(2) Å, *c* = 3.8763(1) Å, Volume = 105.944(4) $Å^3$

Radiation source: Neutron time of flight

Temperature: 300 K

wR = 2.94%; *GOF* = 2.38

Table 2. Structural parameters and crystallographic positions from the refinement of neutron powder diffraction data collected from $H_{0.10}ReO_3$ at 300 K.

Atoms	x/*a*	y/*b*	z/*c*	S.O.F.	U_{iso} equiv. ($Å^2$)
Re1	0	0	0	1	0.00154
Re2	1/2	1/2	0	1	0.00135
O1	0.2707(2)	0.2299(3)	0	1	0.00796
O2	0.2374(1)	0.7335(2)	0	1	0.06365
O3	1/2	1/2	1/2	1	0.03597
O4	0	0	1/2	1	0.05510
H1	1/2	0	1/2	0.102(1)	0.01383
H2	0	1/2	1/2	0.102(1)	0.00012

$H_{0.10}ReO_3$ space group *P*2/*m* (#10)

Formula weight: 234.31 g mol^{-1}, Z = 2

a = 5.3125(1) Å, *b* = 5.3155(3) Å, *c* = 3.7045(3) Å, γ = 90.43(1) °, Volume = 104.609(9) $Å^3$

Radiation source: Neutron time of flight

Temperature: 300 K

wR = 3.475%; *GOF* = 2.34

References

[1] C.J. Raub, A.R. Sweedler, M.A. Jensen, S. Broadston, B.T. Matthias, Superconductivity of Sodium Tungsten Bronzes, Phys. Rev. Lett. 13 (1964) 746–747. https://doi.org/10.1103/PhysRevLett.13.746.

[2] A.R. Sweedler, C.J. Raub, B.T. Matthias, Superconductivity of the alkali tungsten bronzes, Phys. Lett. 15 (1965) 108–109. https://doi.org/10.1016/0031-9163(65)91292-8.

[3] L.E. Conroy, G. Podolsky, Preparation of Tungsten Bronzes from Metal Halides, Inorg. Chem. 7 (1968) 614–615. https://doi.org/10.1021/ic50061a049.

[4] W. Ostertag, Magnetic susceptibility of cubic uranium tungsten bronzes between 4.2 and 560°K, Inorg. Chem. 8 (1969) 1373–1374. https://doi.org/10.1021/ic50076a034.

[5] J. Guo, C. Dong, L. Yang, H. Chen, Crystal structure and superconductivity of rubidium tungsten bronzes Rb_xWO_3 prepared by a hybrid microwave method, Mater. Res. Bull. 43 (2008) 779–786. https://doi.org/10.1016/j.materresbull.2008.01.005.

[6] A.R. Sweedler, J.K. Hulm, B.T. Matthias, T.H. Geballe, Superconductivity of barium tungsten bronze, Phys. Lett. 19 (1965) 82. https://doi.org/10.1016/0031-9163(65)90717-1.

[7] X.L. Xu, H.W. Schmalle, J. R. Günter, Crystal structure of a hexagonal tin tungsten bronze prepared by a mild reaction, Solid State Ionics. 76 (1995) 221–228. https://doi.org/10.1016/0167-2738(94)00281-V.

[8] J.F. Thomas, M.J. Sienko, Low temperature magnetic susceptibility of uranium and rare earth tungsten oxide bronzes, J. Chem. Phys. 61 (1974) 3920–3924. https://doi.org/10.1063/1.1681684.

[9] S.T. Triantafyllou, P.C. Christidis, C.B. Lioutas, An X-ray and electron diffraction study of the intergrowth tungsten bronze $Sb_{0.16}WO_3$, J. Solid State Chem. 134 (1997) 344–348. https://doi.org/10.1006/JSSC.1997.7577.

[10] M.J. Sienko, Thallium-Tungsten Bronze: A Solid State Defect Structure, J. Am. Chem. Soc. 81 (1959) 5556–5559. https://doi.org/10.1021/ja01530a012.

[11] T.E. Gier, D.C. Pease, A.W. Sleight, T.A. Bither, New Lithium, Ammonium, and Tin Hexagonal Tungsten Bronzes Prepared Hydrothermally, Inorg. Chem. 7 (1968) 1646–1647. https://doi.org/10.1021/ic50066a036.

[12] L.H. Cadwell, R.C. Morris, W.G. Moulton, Normal and superconducting properties of K_xWO_3, Phys. Rev. B. 23 (1981) 2219–2223. https://doi.org/10.1103/PhysRevB.23.2219.

[13] Q. Zhong, J.R. Dahn, K. Colbow, Lithium intercalation into WO_3 and the phase diagram of Li_xWO_3, Phys. Rev. B. 46 (1992) 2554–2560. https://doi.org/10.1103/PhysRevB.46.2554.

[14] S.T. Triantafyllou, P.C. Christidis, C.B. Lioutas, An X-ray and electron diffraction study of the tetragonal lead tungsten bronze $Pb_{0.26}WO_3$, J. Solid State Chem. 130 (1997) 176–183. https://doi.org/10.1006/jssc.1997.7577.

[15] P.G. Dickens, R.J. Hurditch, X-ray and neutron diffraction studies of a tetragonal hydrogen bronze H_xWO_3, Nature. 215 (1967) 1266–1267. https://doi.org/10.1038/2151266a0.

[16] F.O. von Rohr, A. Ryser, H. Ji, K. Stolze, J. Tao, J.J. Frick, G.R. Patzke, R.J. Cava, The *h*-Sb_xWO_{3+2x} oxygen excess antimony tungsten bronze, Chem. - A Eur. J. 25 (2019) 2082–2088. https://doi.org/10.1002/chem.201805251.

[17] P.G. Dickens, M.S. Whittingham, The tungsten bronzes and related compounds, Q. Rev. Chem. Soc. 22 (1968) 30–44. https://doi.org/10.1039/qr9682200030.

[18] N.D. Zakharov, P. Werner, I.P. Zibrov, V.P. Filonenko, M. Sundberg, Structural studies of calcium tungsten bronzes, Ca_xWO_3, formed at high pressure, Cryst. Res. Technol. 35 (2000) 713–720. https://doi.org/10.1002/1521-4079(200007)35:6/7<713::AID-CRAT713>3.0.CO;2-Z.

[19] A. Benmoussa, D. Groult, F. Studer, B. Raveau, Intergrowth of hexagonal tungsten bronze and perovskite-like structures: The oxides $ACu_3M_7O_{21}$ (A = K, Rb, Cs, TI; M = Nb, Ta), J. Solid State Chem. 41 (1982) 221–226. https://doi.org/10.1016/0022-4596(82)90205-5.

[20] M.J. Sienko, Electric and Magnetic Properties of the tungsten and vanadium bronzes, Advances in Chemistry, 39 (1963) 224-236. https://pubs.acs.org/doi/10.1021/ba-1964-0039.ch021.

[21] M. Safrany Renard, N. Emery, E.M. Roginskii, R. Baddour-Hadjean, J.P. Pereira-Ramos, Crystal structure determination of a new sodium vanadium bronze electrochemically formed, J. Solid State Chem. 254 (2017) 62–68. https://doi.org/10.1016/j.jssc.2017.07.012.

[22] D. Ridgley, R. Ward, The Preparation of a strontium-niobium bronze with the perovskite structure, J. Am. Chem. Soc. 77 (1955) 6132–6136. https://doi.org/10.1021/ja01628a011.

[23] R.R. Kreiser, R. Ward, The preparation of a barium niobium bronze, J. Solid State Chem. 1 (1970) 368–371. https://doi.org/10.1016/0022-4596(70)90117-9.

[24] A. Wold, W. Kunnmann, R.J. Arnott, A. Ferretti, Preparation and properties of sodium and potassium molybdenum bronze crystals, Inorg. Chem. 3 (1964) 545–547. https://doi.org/10.1021/ic50014a022.

[25] N.C. Stephenson, A.D. Wadsley, The crystal structure of the red potassium molybdenumbronze, $K_{0.26}MoO_3$, Acta Crystallogr. 19 (1965) 241–247. https://doi.org/10.1107/s0365110x65005121.

[26] W.J. Schutte, J.L. De Boer, The incommensurately modulated structures of the blue bronzes $K_{0.3}MoO_3$ and $Rb_{0.3}MoO_3$, Acta Crystallogr. Sect. B. 49 (1993) 579–591. https://doi.org/10.1107/S0108768192006578.

[27] J. Graham, A.D. Wadsley, The crystal structure of the blue potassium molybdenum bronze, $K_{0.28}MoO_3$, Acta Crystallogr. 20 (1966) 93–100. https://doi.org/10.1107/s0365110x66000173.

[28] P.G. Dickens, M.T. Weller, The structure of a cubic hydrogen rhenium bronze, $H_{1.36}Re0_3$,

J. Solid State Chem. 48 (1983) 407–411. https://doi.org/10.1016/0022-4596(83)90099-3.

[29] M.T. Weller, P.G. Dickens, Studies of some hydrogen rhenium bronzes, Solid State Ionics. 9–10 (1983) 1081–1085. https://doi.org/10.1016/0167-2738(83)90134-0.

[30] J.J. Birtill, P.G. Dickens, Phase relationships in the system H_xMoO_3 ($0<x\leq2.0$), Mater. Res. Bull. 13 (1978) 311–316. https://doi.org/10.1016/0025-5408(78)90008-9.

[31] N. Kimizuka, T. Akahane, S. Matsumoto, K. Yukino, Synthesis and some crystal data of H_xReO_3 (x = 0.15), Inorg. Chem. 15 (1976) 3178–3179. https://doi.org/10.1021/ic50166a053.

[32] C. Janáky, K. Rajeshwar, N.R. de Tacconi, W. Chanmanee, M.N. Huda, Tungsten-based oxide semiconductors for solar hydrogen generation, Catal. Today. 199 (2013) 53–64. https://doi.org/10.1016/J.CATTOD.2012.07.020.

[33] C.G. Granqvist, Electrochromic tungsten oxide films : Review of progress 1993 - 1998, Sol. Energy Mater. Sol. Cells. 60 (2000) 201–262.

[34] L. Tegg, D. Cuskelly, V.J. Keast, The sodium tungsten bronzes as plasmonic materials: fabrication, calculation and characterization, Mater. Res. Express. 4 (2017) 065703. https://doi.org/10.1088/2053-1591/aa6c40.

[35] S.K. Deb, Opportunities and challenges in science and technology of WO_3 for electrochromic and related applications, Sol. Energy Mater. Sol. Cells. 92 (2008) 245–258. https://doi.org/10.1016/J.SOLMAT.2007.01.026.

[36] M.J. Sienko, S.M. Morehouse, Electrical and magnetic properties of potassium tungsten bronze and rubidium tungsten bronze, Inorg. Chem. 2 (1963) 485–489. https://doi.org/10.1021/ic50007a014.

[37] H.R. Shanks, Enhancement of the superconducting transition temperature near a phase instability in Na_xWO_3, Solid State Commun. 15 (1974) 753–756. https://doi.org/10.1016/0038-1098(74)90254-3.

[38] J.P. Remeika, T.H. Geballe, B.T. Matthias, A.S. Cooper, G.W. Hull, E.M. Kelly, Superconductivity in hexagonal tungsten bronzes, Phys. Lett. A. 24 (1967) 565–566. https://doi.org/10.1016/0375-9601(67)90616-0.

[39] J.E. Ostenson, H.R. Shanks, D.K. Finnemore, Superconductivity in the tungsten bronzes, J. Less-Common Met. 62 (1978) 149–153. https://doi.org/10.1016/0022-5088(78)90024-3.

[40] N.N. Garif'yanov, S.Y. Khlebnikov, I.S. Khlebnikov, I.A. Garifullin, Superconductivity of sodium tungsten bronze with cubic structure, Czechoslov. J. Phys. 46 (1996) 855–856. https://doi.org/10.1007/BF02583735.

[41] J.D. Bocarsly, D. Hirai, M.N. Ali, R.J. Cava, Superconducting phase diagram of In_xWO_3 synthesized by indium deintercalation, Epl. 103 (2013). https://doi.org/10.1209/0295-5075/103/17001.

[42] R. Brusetti, P. Bordet, J. Bossy, H. Schober, S. Eibl, Superconductivity in the tungsten bronze Rb_xWO_3 ($0.20\leq x\leq0.33$) in connection with its structure, electronic density of

states, and phonon density of states, Phys. Rev. B - Condens. Matter Mater. Phys. 76 (2007) 1–15. https://doi.org/10.1103/PhysRevB.76.174511.

[43] N. Haldolaarachchige, Q. Gibson, J. Krizan, R.J. Cava, Superconducting properties of the K_xWO_3 tetragonal tungsten bronze and the superconducting phase diagram of the tungsten bronze family, Phys. Rev. B - Condens. Matter Mater. Phys. 89 (2014) 1–6. https://doi.org/10.1103/PhysRevB.89.104520.

[44] R. Fan, X.H. Chen, Z. Gui, Z. Sun, S.Y. Li, Z.Y. Chen, Chemical synthesis and electronic conduction properties of sodium and potassium tungsten bronzes, J. Phys. Chem. Solids. 61 (2000) 2029–2033. https://doi.org/10.1016/S0022-3697(00)00202-X.

[45] L. Jin, S. Guo, R.J. Cava, $Sn_{0.24}WO_3$ hexagonal tungsten bronze prepared via the metal chloride route, J. Solid State Chem. 291 (2020) 121553. https://doi.org/10.1016/j.jssc.2020.121553.

[46] L.E. Conroy, T. Yokokawa, The preparation and properties of a barium tungsten bronze, Inorg. Chem. 4 (1965) 994–996. https://doi.org/10.1021/ic50029a015.

[47] D. Hirai, E. Climent-Pascual, R.J. Cava, Superconductivity in $WO_{2.6}F_{0.4}$ synthesized by reaction of WO_3 with teflon, Phys. Rev. B - Condens. Matter Mater. Phys. 84 (2011) 2–7. https://doi.org/10.1103/PhysRevB.84.174519.

[48] P.J. Wiseman, P.G. Dickens, The crystal structure of cubic hydrogen tungsten bronze, J. Solid State Chem. 6 (1973) 374–377. https://doi.org/10.1016/0022-4596(73)90225-9.

[49] O. Glemser, C. Naumann, Kristallisierte Wolframblauverbindungen; Wasserstoffanaloga der Wolframbronzen H_xWO_3, Z. Anorg. Allg Chem. 265 (1951) 288–302. https://doi.org/10.1002/zaac.19512650413.

[50] S. Horiuchi, N. Kimizuka, A. Yamamoto, Absorption of hydrogen in "ReO_3," Nature. 279 (1979) 226–227. https://doi.org/10.1038/279226a0.

[51] F. Takusagawa, R.A. Jacobson, Crystal structure studies of tetragonal sodium tungsten bronzes, Na_xWO_3. I. $Na_{0.33}WO_3$ and $Na_{0.48}WO_3$, J. Solid State Chem. 18 (1976) 163–174. https://doi.org/10.1016/0022-4596(76)90092-X.

[52] S.T. Triantafyllou, P.C. Christidis, C.B. Lioutas, X-ray and electron diffraction study of the tetragonal sodium tungsten bronze, $Na_{0.10}WO_3$, with distorted perovskite structure, J. Solid State Chem. 133 (1997) 479–485. https://doi.org/10.1006/jssc.1997.7513.

[53] B.W. Brown, E. Banks, The sodium tungsten bronzes, J. Am. Chem. Soc. 76 (1954) 963–966. https://doi.org/10.1021/ja01633a004.

[54] P.J. Wiseman, P.G. Dickens, Neutron diffraction studies of cubic tungsten bronzes, J. Solid State Chem. 17 (1976) 91–100. https://doi.org/10.1016/0022-4596(76)90206-1.

[55] M.E. Straumanis, The sodium tungsten bronzes. I. chemical properties and structure, J. Am. Chem. Soc. 71 (1949) 679–683. https://doi.org/10.1021/ja01170a085.

[56] S. Paul, G.D. Mukherjee, A. Ghosh, S. Oishi, S. Raj, Temperature dependent X-ray diffraction study of lightly doped Na_xWO_3, Appl. Phys. Lett. 98 (2011) 121910.

https://doi.org/10.1063/1.3569716.

[57] M.S. Rahman, M.M. Murshed, T.M. Gesing, Synthesis, characterization and time dependent phase transformation of $Li_{0.4}WO_3$ bronze, Zeitschrift Fur Krist. - Cryst. Mater. 229 (2014) 797–805. https://doi.org/10.1515/zkri-2014-1777.

[58] M.E. Straumanis, G.F. Doctor, The system sodium tungsten bronze-lithium tungsten bronze-tungsten(VI) oxide, J. Am. Chem. Soc. 73 (1951) 3492–3496. https://doi.org/10.1021/ja01151a147.